Supplementary Information

Electrospun PVA-Chitosan Nanofibers with Antibacterial Properties for Wound Healing: Unveiling the Potential of Low Molecular Weight Chitosan

Table of Content

Fig. S1 ^{1}H A) and ^{13}C B) NMR spectra of CS7 (blue line) and CS1 (green line).

Fig. S2 Characterization of **CS300** (red line), **CS7** (blue line) and **CS1** (green line). A) UV-vis spectra of **CS300**, **CS7** and **CS1** at pH 5.5 (1 mg/mL). B) Water solubility of **CS300**, **CS7** and **CS1** with pH in the pH range 4-12 at 0.2 w/v%.

Fig. S3. pKa estimation of CS samples. A) Derivative of the ζ-potential distribution at different pH values and B) the relationship between the calculated Molecular Weight (MW) and the pKa.

Fig. S4 Morphology and diameter statistics of pure PVA NFs. A) Representative SEM image of PVA NFs. B) Diameter analysis of PVA NFs.

Fig. S5 Dimensional analysis of PVA@CS1 NFs and PVA@CS7 NFs (200 nanofibers). A) PVA@CS1-1, B) PVA@CS7-1, C) PVA@CS1-2, D) PVA@CS7-2, E) PVA@CS1-3, F) PVA@CS7-3, G) PVA@CS1-4, H) PVA@CS7-4, I) PVA@CS1-5, and J) PVA@CS7-5.

Fig. S6 Electrical conductivity and dynamic viscosity characterization of PVA@CS1 and PVA@CS7 electrospinning solutions. (A, B) Electrical conductivity as a function of CS content for the PVA@CS1 and PVA@CS7 series, respectively. (C, D) Dynamic viscosity as a function of CS content for the PVA@CS1 and PVA@CS7 solutions, respectively. The dynamic viscosity of PVA@CS1 solutions decreases with increasing CS content, whereas that of PVA@CS7 solutions increases gradually as CS content increases.

Fig. S7. A) Comparison of FTIR spectra of PVA NFs, PVA@CS1-1~5 and **CS1**. B) Comparison of UV-vis spectra of PVA NFs, PVA@CS1-1~5 and **CS1**. C) Comparison of FTIR spectra of PVA NFs, PVA@CS7-1~5 and CS7. D) Comparison of UV-vis spectra of PVA NFs, PVA@CS7-1~5 and **CS7**.

Fig. S8. Schematic representation of possible accumulation of CS molecules at the surface of the PVA NFs produced higher percentages of **CS1** and **CS7**.

Fig. S9. Calibration lines obtained from NMR studies for A) PVA, B) **CS7** and C) **CS1**.

Fig. S10. UV-vis spectra of CS release from PVA@CS NFs in water at different time points. (A)PVA@CS1-2; (B) PVA@CS1-5;(C) PVA@CS7-2;(D) PVA@CS7-5.

Fig. S11. Measurements of cell density (optical density at 600 nm, OD600) of A) *S. aureus* (ATCC 12600), B) *E. coli* (K12) and C) *P. aeruginosa* (PA01) in LB as a function of PVA, **CS300**, **CS7** and **CS1** concentration. The cultures were incubated at 37 ^{o}C for 18 h before the measurements. Depicted values (average ± SD) are based on 3 biological replicas.

Fig. S12. Measurements of cell density (optical density at 600 nm, OD600) of *C. albicans* (ATCC 10231) in A) Sabouraud (pH 5.5) and B) LB (pH 7.4) media as a function of PVA, **CS300**, **CS7** and **CS1** concentration. The cultures were incubated at 37 ^{o}C for 18 h before the measurements. Depicted values (average ± SD) are based on 3 biological replicas.

Fig. S13. Representative images of PVA@CS7 NF disks incubated overnight in agar previously inoculated with *E. coli* (K12).

Fig. S14. Weight distribution of A) PVA@CS1 and B) PVA@CS7 NFs disks for microbial detection and estimated release from C) **CS7** or D) **CS1**.

Fig. S15. Representative images of HaCaT-ras A5 cells proliferation in the presence of PVA, **CS1**, and **CS7** at different concentrations (scale bar = 100 μm).

Fig. S16. Representative images of HaCaT-ras A5 cells proliferation in the absence (untreated) and in the presence of PVA and PVA@CS7 NF (scale bar = 100 μm).

Fig. S17. Schematic representation for the fabrication of the NFs by the electrospinning including photographic images of the electrospinning process after 15 and 60 min.

1 SUPPORTING EXPERIMENTAL CONTENT

1.1 Determination of the elemental nitrogen content in CS7 and CS1 and the encapsulation efficiency in PVA@CS NFs

The nitrogen content of CS was estimated from the degree of deacetylation (DD) determined by NMR, resulting in a theoretical nitrogen percentage of 8.18% for both **CS1** and **CS7**. For nanofiber composites, the theoretical nitrogen fraction was calculated based on the feed ratios of CS and PVA in the electrospinning solutions. Experimental nitrogen content was obtained from elemental analysis of electrospun fibers. The ratio between experimental and theoretical values ($CS_{Exp}/CS_{Theo}\cdot 100$) was defined as the encapsulation efficiency (EE). Table S1 summarizes the input masses of PVA, **CS1**, and **CS7**, the theoretical and experimental nitrogen contents, and the calculated CS incorporation into nanofibers.

The calculation of nitrogen (N) content is based on its chemical composition and degree of deacetylation (DD). Chitooligosaccharides (CS) are composed of D-glucosamine (GlcN) and N-acetylglucosamine (GlcNAc) units, where nitrogen is only derived from amino ($-NH_2$) and acetylamino ($-NHCOCH_3$) groups.

COS is an oligomer of chitosan, and the chemical structure can be expressed as:

$(C_6H_{11}NO_4)_m\,(C_8H_{13}NO_5)_n$

m denotes the number of moles of D-glucosamine unit (GlcN).

n denotes the number of moles of N-acetylglucosamine unit (GlcNAc).

The total number of units is: $m + n = N_{\text{total}}$.

The calculation of the nitrogen content needs to be combined with the degree of deacetylation (DD) of chitosan, since DD determines the *m* and *n* ratio.

The average molar mass of the chemical formula for chitosan is:

$$M_{\text{Average chitosan}} = DD \cdot M_{\text{GlcN}} + (1 - DD) \cdot M_{\text{GlcNAc}}$$

M_{GlcN} =161.16g/mol (Molar mass of D-glucosamine)

M_{GlcNAc} =203.19g/mol (Molar mass of N-acetylglucosamine)

Nitrogen content (mass percent) was:

$$\omega(N) = \frac{M_N}{DD \cdot M_{GlcN} + (1 - DD) \cdot M_{GlcNAc}} \times 100\%$$

DD is 75.8% for **CS7** and 76.6% for **CS1**, based on NMR test results (see Section 2.1)

$M_{\text{Average chitosan}}$ (7KDa) = 75.8% x 161.16 + (1-75.8%) x 203.19 = 171.33 g/mol

$$\omega(N) = \frac{14.01}{171.33} \times 100\% = 8.18\%$$

$M_{\text{Average chitosan}}$ (1KDa) = 76.6% x 161.16 + (1-76.6%) x 203.19 = 171.00 g/mol

$$\omega(N) = \frac{14.01}{171.00} \times 100\% = 8.18\%$$

1.2 Calculation of theoretical mass and theoretical percentage of N, experimental mass, experimental percentage of nitrogen, experimental percentage of CSs and EE for PVA@NFs

$$(mass\ of\ N)_{Theor} = \frac{(mass\ of\ CS)_{Theor}\ x\ 8.18}{100}$$

$$(\%\ of\ N)_{Theor} = \frac{(mass\ of\ N)_{Theor}\ x\ 100}{mass\ of\ NFs}$$

$$(mass\ of\ N)_{Exp} = \frac{(\%\ of\ N)_{Exp}\ x\ mass\ of\ NFs}{100}$$

$$(mass\ of\ CS)_{Exp} = \frac{(mass\ of\ N)_{Exp}\ x\ 100}{8.18}$$

$$(\%\ of\ CS)_{Exp} = \frac{(\%\ of\ N)_{Exp}\ x\ 8.18}{100}$$

$$EE = \frac{CS_{Exp}}{CS_{Theor}} \cdot 100$$

1.3 Molecular weight determination via diffusion NMR

During the NMR analysis, the diffusion time (Δ) varied between 100 and 150 milliseconds, while the gradient pulse duration (δ) ranged from 1.75 to 3 milliseconds. Gradient strengths were incrementally increased by 4%, starting from 8% and reaching up to 96%, resulting in 23 data points for each inversion Laplace transform (ILT) analysis. A consistent recovery delay of

5 seconds was maintained to allow the system to return to equilibrium between scans. Each gradient increment involved 96 scans, leading to typical experimental durations of about 8 hours per sample. All measurements were conducted without sample rotation to avoid any disturbances that could affect diffusion.

To ensure reproducibility and to minimize convection effects, which can affect diffusion measurements, three separate experiments were performed using different Δ values, as recommended in previous studies.[103] The diffusion coefficients calculated from these experiments remained consistent across the different diffusion times tested, indicating that convection had a negligible impact on the results.

Diffusion experiments were performed using a Bruker Avance III HD 500 NMR spectrophotometer. Diffusion measurements employed the Pulsed Gradient Stimulated Echo (PGSE) sequence combined with bipolar gradient pulses.[104] Smoothed rectangular (SMSQ) gradient pulses were used, which were adjusted in strength throughout the experiments to provide precise control of nuclear spin encoding. Moreover, the use of SMSQ gradient pulses enhances the accuracy of the diffusion measurements by reducing eddy current effects and improving the uniformity of the gradient field. The combination of PGSE with bipolar gradients further minimizes systematic errors, making this method highly suitable for studying polymers and biopolymers like chitooligosaccharide. The diffusion coefficients (D values) were extracted from the slope of the regression line plotting Ln(I/I0) against G^2. This regression approach linearizes the ILT based on the Stejskal-Tanner equation for SMSQ gradient pulses (Eq. 1),[105] where I/I0 represents the ratio of the observed spin echo intensity to the intensity without gradients, G is the gradient strength, Δ is the delay between the midpoints of the gradient pulses, D is the diffusion coefficient, δ is the gradient duration, τ is the delay in recovery of the gradient and the duration of the 180º pulse.

$$\ln\left(\frac{I}{I_0}\right) = -(\gamma\delta)^2\left(\Delta - \frac{6.344\pi^2 - 207}{19.44\pi^2}\delta - \frac{\tau}{2}\right)D\frac{81}{100}G^2 \quad (1)$$

Least Mean Squares (LMS) fittings were performed using the DiffAtOnce software package, a registered program developed by some of us (ref). This software facilitated advanced analysis of diffusion NMR data by implementing sophisticated algorithms for inverse Laplace transform (ILT) calculations. The Stejskal-Tanner equation, previously referenced as Equation 1, can be reformulated into an improper integral equation known as the Laplace transform (LT), presented here as Equation 2. This transformation effectively converts the diffusion coefficient distribution from the diffusion domain to the Laplace domain, allowing for the extraction of

A(D) by performing an inverse Laplace transformation on the experimental data. The adjusted diffusion time Δ' is particularly significant, as it accounts for the specifics of the pulse sequence parameters, ensuring accurate modeling of the diffusion process.

$$L\{A(D)\} = \int_0^\infty A(D) e^{-(\gamma\delta)^2 G^2 D\Delta'} dD \quad (2)$$

To obtain a continuous distribution of D-values (A(D)) from Eq. 2 a non-linear ILT must be performed. Various algorithms were applied. DART solutions were obtained using an algebraic reconstruction technique as described in reference.[106] This iterative method reconstructs the diffusion coefficient distribution by minimizing the difference between the experimental data and the model, subject to constraints that promote stability and convergence. TRAIn solutions were obtained using the algorithm provided by Xu et al. (2014) [107] with a sparsity parameter set to 1.05. Both methods utilized the Hilbert space framework derived from the exponential kernel of the Laplace transform. By operating within this mathematical space, the algorithms effectively managed the complexities of the ILT, leading to more accurate and reliable diffusion coefficient distributions. Additionally, Diffusion Ordered Spectroscopy (DOSY) were generated using the Sparse and Low Rank Alternating Direction Unmixing algorithms (ADSpLRU) reported by Giampouras et al. (2016).[108] This approach was applied for the first time to the resolution of DOSY maps by Yuan et al. (2017) [109] (SILT-DOSY). The ADSpLRU algorithm enhances the separation of overlapping signals in DOSY spectra by exploiting the sparsity and low-rank structure inherent in the data, leading to improved resolution and quantification of individual components in complex mixtures.

By applying Eq. 1 and Eq. 2, the diffusion coefficients obtained can be directly correlated with the molecular weights of the oligochitosan samples according to Arrabal-Campos et al. (2016).[110] The relationship between diffusion coefficients and molecular weights is based on a solvent-independent universal calibration curve. This curve, in combination with SILT-DOSY, allows the transformation of D values into Mw estimations, creating a new type of Molecular Weight-Ordered SpectroscopY (MwOSY). This allows for the estimation of molecular weights and distributions in solution, providing valuable insights into the physical and chemical properties of the oligochitosan being studied.

1.4 Release experiments

For the quantification of the release **CS7**, **CS1** and PVA, firstly, three different calibration lines were prepared, one for the obtained **CS7** and **CS1** by microwave irradiation, and another with PVA. To obtain these three calibration lines, precise quantities of 1, 2, 4, 6, 8, and 10 mg of **CS7**, CS and PVA were weighed, and then, they were dissolved in 1 mL of D_2O. In the case of the CS samples, it was necessary to sonicate the samples for 10 minutes to ensure complete dissolution. After that, a 1:4 dilution of each sample was made, finally transferring 500 µL of the resulting solution to an NMR tube for measurement. Concerning the PVA samples, for the calibration line they were heated at 80 °C for 60 minutes, and once complete dissolution was achieved, they were allowed to cool down to room temperature. Then, 500 µL of the solution was transferred to an NMR tube, ensuring that the temperature and homogeneity of the samples were suitable for analysis. (The calibration line is shown in **Fig. S9**). The Bruker 1D noesygppr1d pulse sequence was used, which consists of a presaturation pulse for suppression of the residual H_2O signal. The acquisition parameters were the following: dummy scans (DS) = 4, number of scans (NS) = 32, FID size (TD) = 66K, spectral width (SW) = 20.0 ppm, acquisition time (AQ) = 2.73 s, recycle time (D1) = 10 s, receiver gain (RG) = 91, FID resolution (FIDRES) = 0.37 Hz and mixing time (D8) = 10 ms. The resulting proton spectra were automatically phase- and baseline-corrected, and all spectra were calibrated to the ERETIC signal by assigning a value of -1 ppm to its singlet. Locking was performed using the deuterium signal from deuterated water (D_2O).

2. SUPPORTING TABLES

Table S1. Summary of the weight percent release of **CS1**, **CS7**, and PVA from PVA@CS1 and PVA@CS7 after 24 hours, quantified by ^{1}H NMR spectroscopy. CS and PVA release efficiency and CS mass released per mg of NFs.

	CS Released [wt. %]	PVA Released [wt. %]	CS Release efficiency* [%]	PVA Release efficiency [%]	CS Released per mg NF [µg]
PVA@CS1-1	4.64	83.92	78.64	89.18	46.40
PVA@CS1-2	9.76	72.90	87.93	82.01	97.60
PVA@CS1-3	14.42	67.92	91.27	80.65	144.20
PVA@CS1-4	18.82	63.20	94.1	79.00	188.20
PVA@CS1-5	23.78	56.50	99.92	74.16	237.80
PVA@CS7-1	4.34	79.40	73.56	84.38	43.40
PVA@CS7-2	9.14	67.66	82.34	76.12	91.40
PVA@CS7-3	14.84	61.68	93.92	73.25	148.40
PVA@CS7-4	19.96	53.04	99.80	66.30	199.60
PVA@CS7-5	21.28	51.14	89.41	67.12	212.80

**Efficiencies are evaluated according to the experimental CS or PVA amounts (Table S1).*

Table S2. Minimal Inhibitory Concentration (MIC) values (mg/mL) of PVA, **CS300**, **CS7** and **CS1** for *C. albicans* (ATCC 10231) determined by the 2-fold dilution method at 37 °C under mild shaking in LB media. Depicted results are based on three biological replicas.

Name	*C. albicans*
PVA	> 30
CS300	15
CS7	7.5
CS1	15

Table S3. Amount of PVA, CS and milliliters of DMF, AcOH (20%, v/v) and H_2O used for fabrication of the PVA NFs, PVA@CS1-1~5 NFs and PVA@CS7-1~5 NFs

Sample name	PVA [mg]	CS [mg]	DMF [ml]	AcOH (20%, v/v) [ml]	H_2O [ml]
PVA NFs	1600	0	0.5	0	9.5
PVA@CS1-1	1600	100	0.5	0.5	9
PVA@CS1-2	1600	200	0.5	0.5	9
PVA@CS1-3	1600	300	0.5	0.5	9
PVA@CS1-4	1600	400	0.5	0.5	9
PVA@CS1-5	1600	500	0.5	0.5	9
PVA@CS7-1	1600	100	0.5	0.5	9
PVA@CS7-2	1600	200	0.5	0.5	9
PVA@CS7-3	1600	300	0.5	0.5	9
PVA@CS7-4	1600	400	0.5	0.5	9
PVA@CS7-5	1600	500	0.5	0.5	9

3. SUPPORTING FIGURES

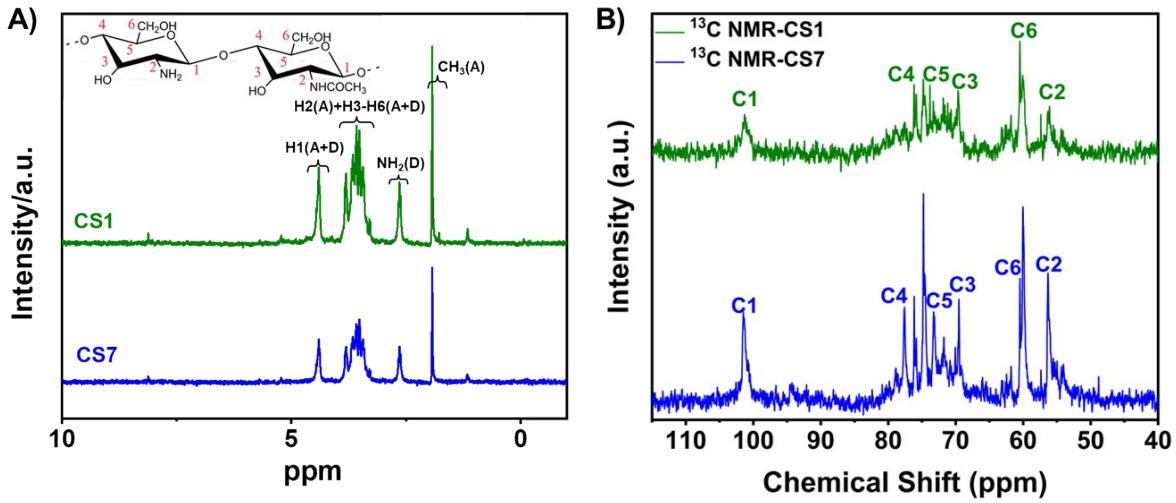

Fig. S1 ^{1}H A) and ^{13}C B) NMR spectra of CS7 (blue line) and CS1 (green line).

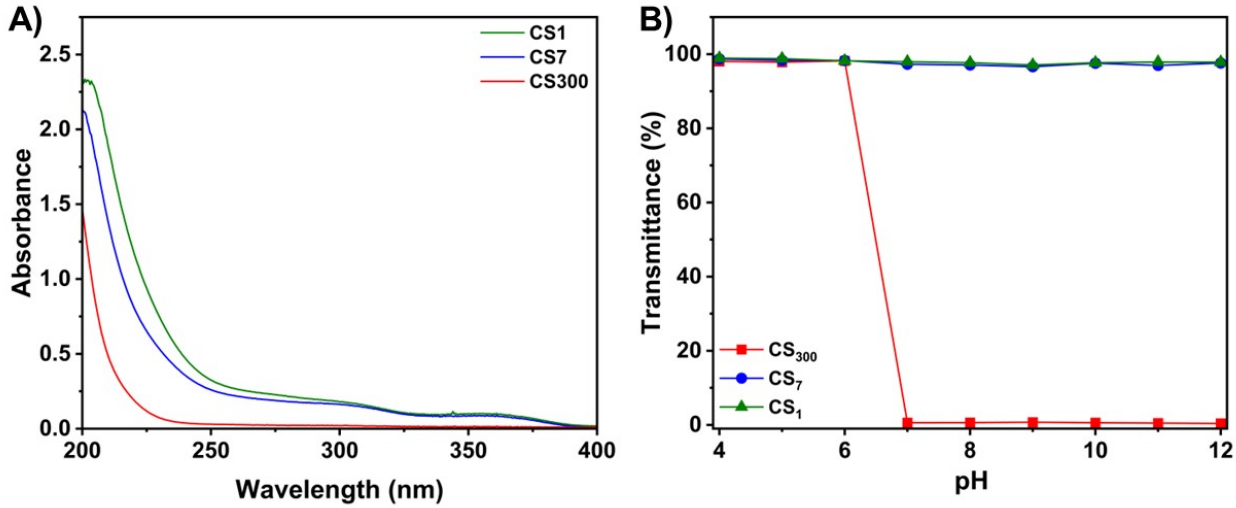

Fig. S2 Characterization of **CS300** (red line), **CS7** (blue line) and **CS1** (green line). A) UV-vis spectra of **CS300**, **CS7** and **CS1** at pH 5.5 (1 mg/mL). B) Water solubility of **CS300**, **CS7** and **CS1** with pH in the pH range 4-12 at 0.2 w/v%.

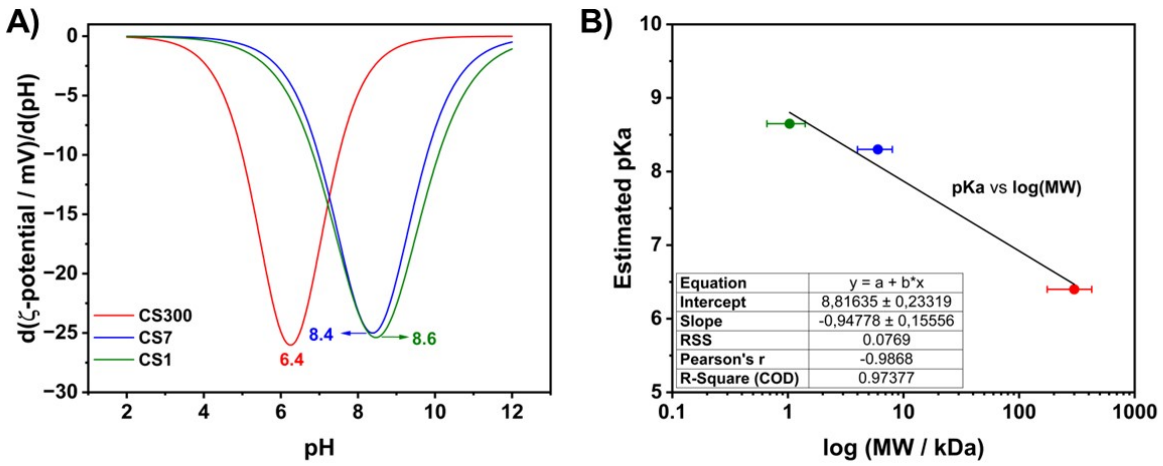

Fig. S3. pKa estimation of CS samples. A) Derivative of the ζ-potential distribution at different pH values and B) the relationship between the calculated Molecular Weight (MW) and the pKa.

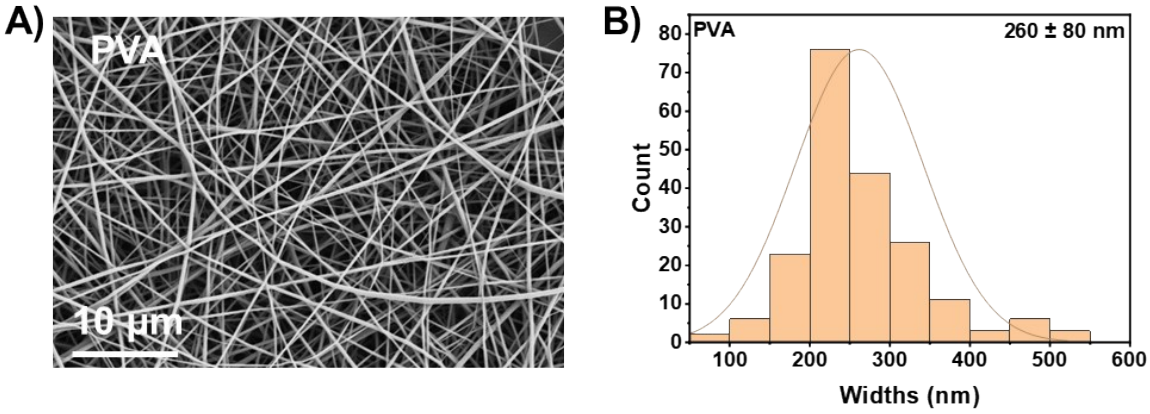

Fig. S4 Morphology and diameter statistics of pure PVA NFs. A) Representative SEM image of PVA NFs. B) Diameter analysis of PVA NFs.

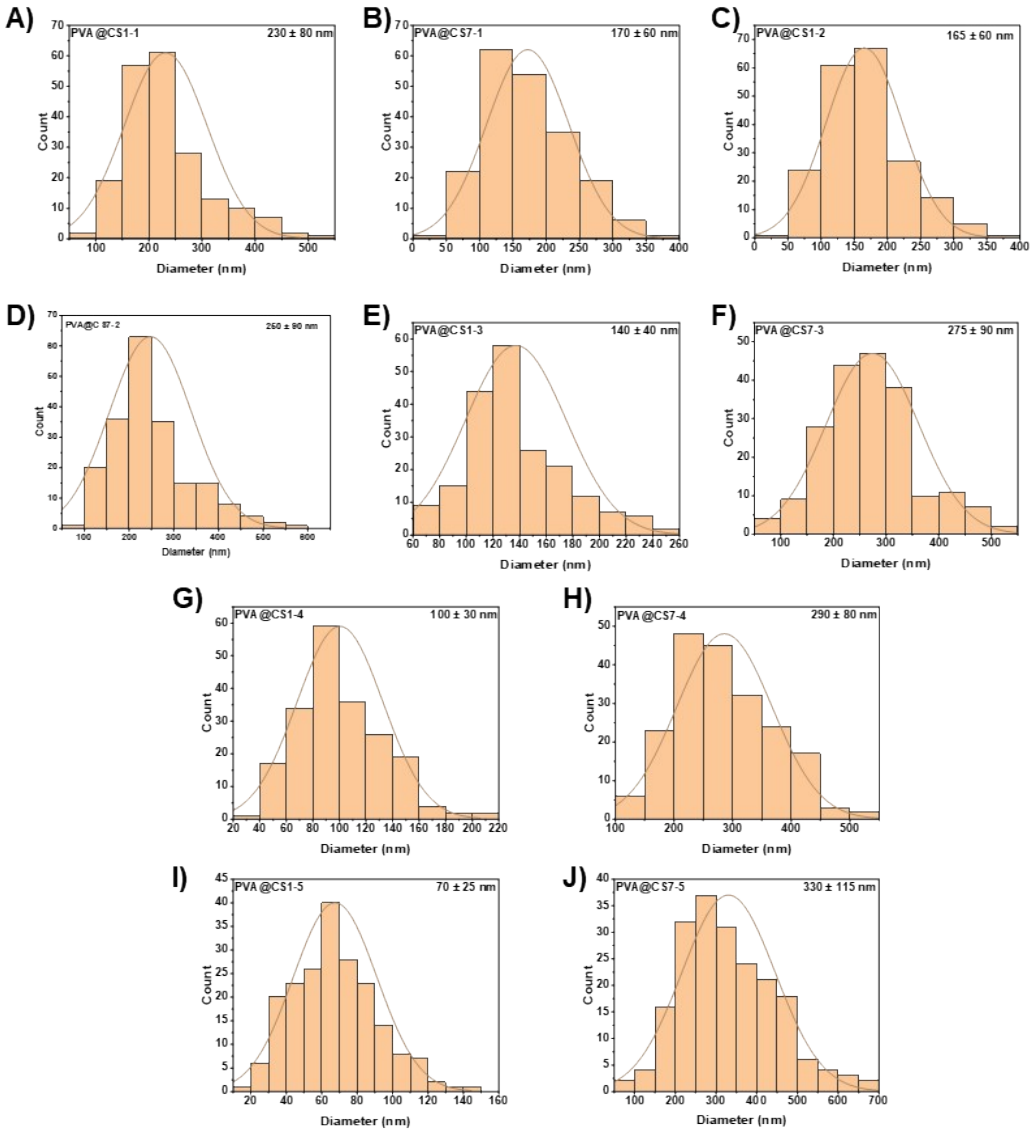

Fig. S5 Dimensional analysis of PVA@CS1 NFs and PVA@CS7 NFs (200 nanofibers). A) PVA@CS1-1, B) PVA@CS7-1, C) PVA@CS1-2, D) PVA@CS7-2, E) PVA@CS1-3, F) PVA@CS7-3, G) PVA@CS1-4, H) PVA@CS7-4, I) PVA@CS1-5, and J) PVA@CS7-5.

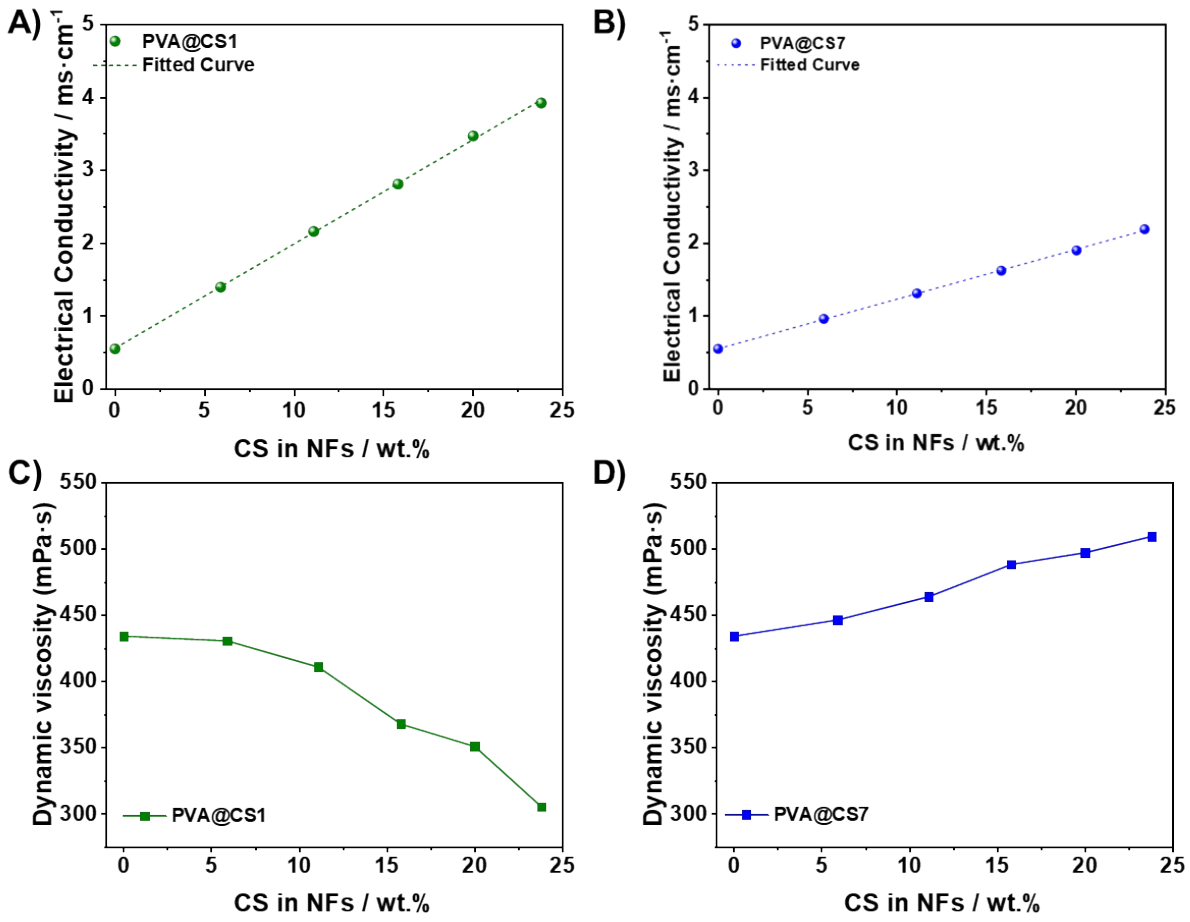

Fig. S6. Electrical conductivity and dynamic viscosity characterization of PVA@CS1 and PVA@CS7 electrospinning solutions. (A, B) Electrical conductivity as a function of CS content for the PVA@CS1 and PVA@CS7 series, respectively. (C, D) Dynamic viscosity as a function of CS content for the PVA@CS1 and PVA@CS7 solutions, respectively. The dynamic viscosity of PVA@CS1 solutions decreases with increasing CS content, whereas that of PVA@CS7 solutions increases gradually as CS content increases.

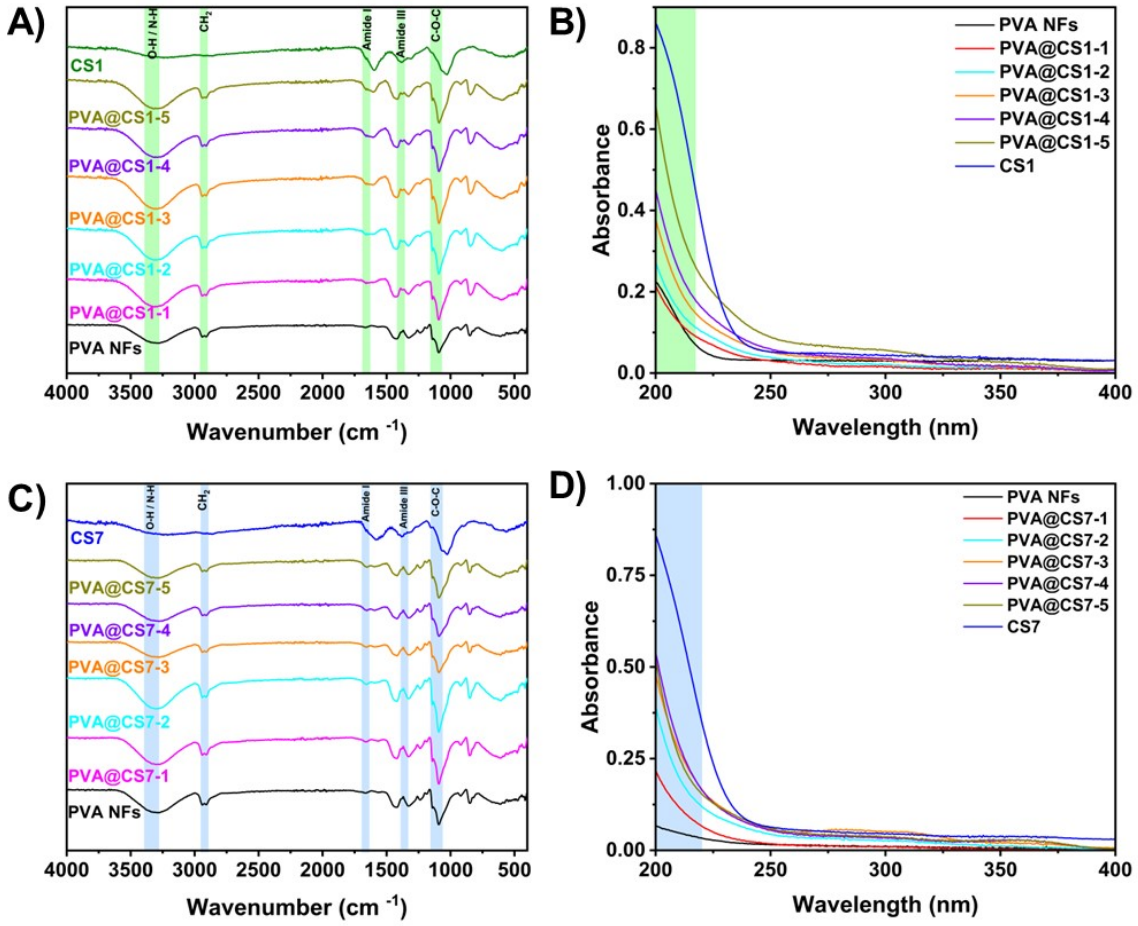

Fig. S7. A) Comparison of FTIR spectra of PVA NFs, PVA@CS1-1~5 and **CS1**. B) Comparison of UV-vis spectra of PVA NFs, PVA@CS1-1~5 and CS1. C) Comparison of FTIR spectra of PVA NFs, PVA@CS7-1~5 and **CS7**. D) Comparison of UV-vis spectra of PVA NFs, PVA@CS7-1~5 and **CS7**.

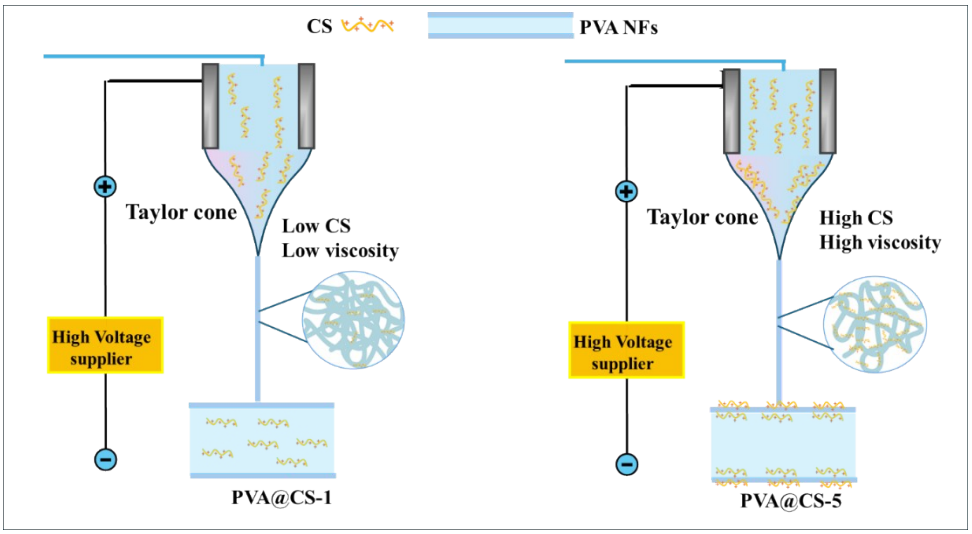

Fig. S8. Schematic representation of possible accumulation of CS molecules at the surface of the PVA NFs produced at higher percentages of **CS1** and **CS7**.

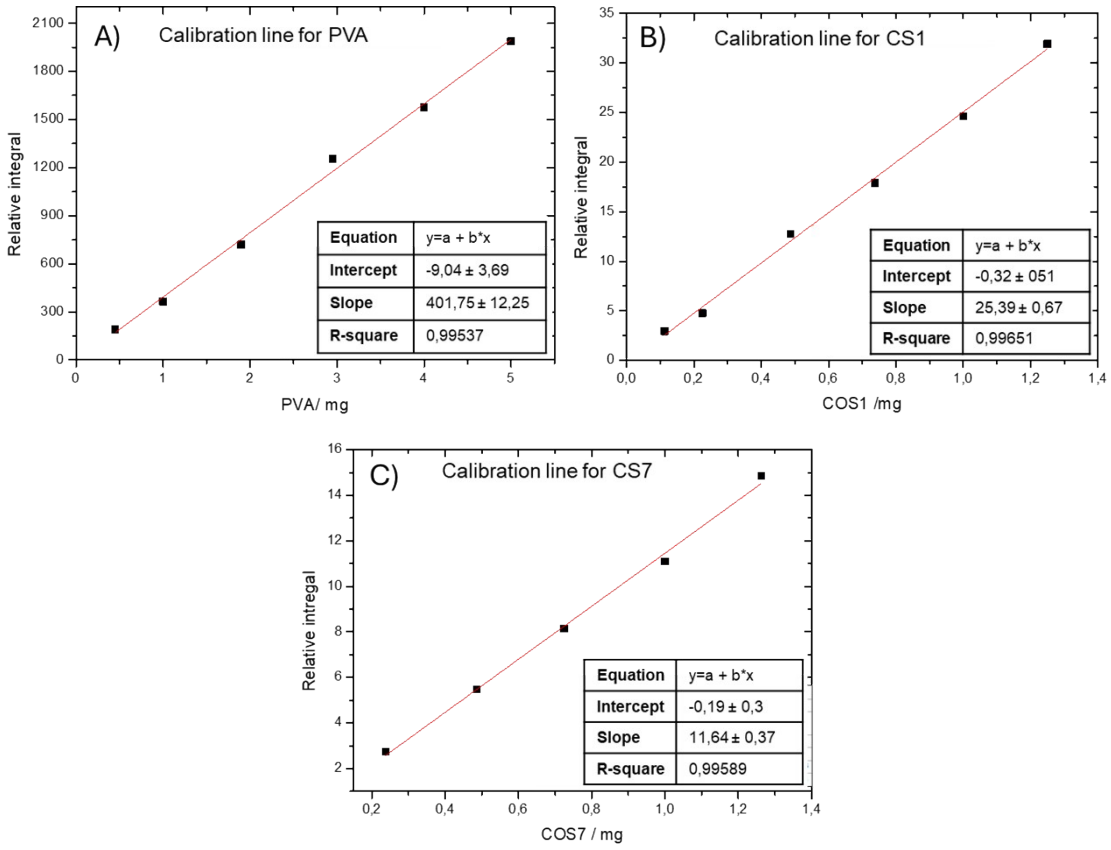

Fig. S9. Calibration lines obtained from NMR studies for A) PVA, B) **CS7** and C) **CS1**.

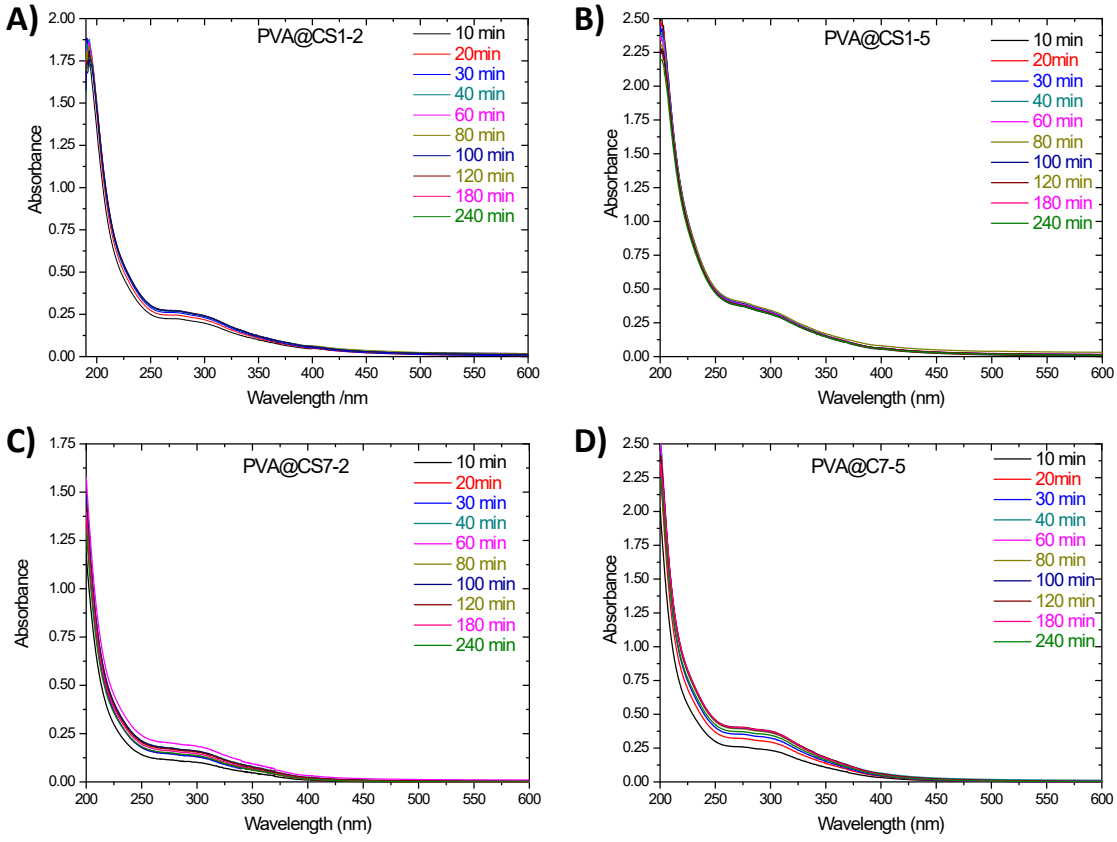

Fig. S10. UV-vis spectra of CS release from PVA@CS NFs in water at different time points. (A)PVA@CS1-2; (B) PVA@CS1-5;(C) PVA@CS7-2;(D) PVA@CS7-5.

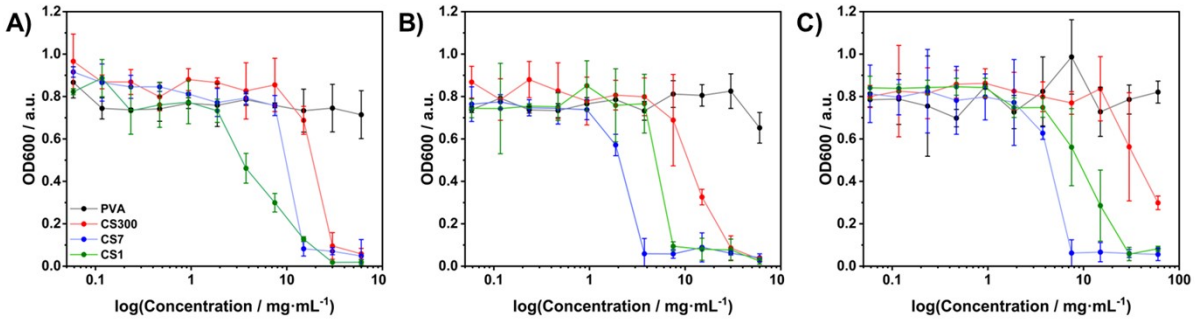

Fig. S11. Measurements of cell density (optical density at 600 nm, OD600) of A) *S. aureus* (ATCC 12600), B) *E. coli* (K12) and C) *P. aeruginosa* (PA01) in LB as a function of PVA, **CS300**, **CS7** and **CS1** concentration. The cultures were incubated at 37 °C for 18 h before the measurements. Depicted values (average ± SD) are based on 3 biological replicas.

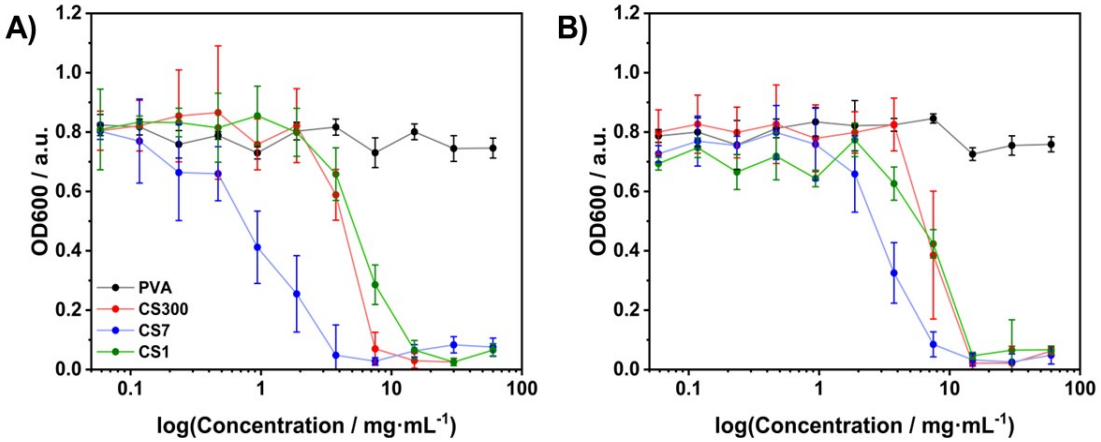

Fig. S12. Measurements of cell density (optical density at 600 nm, OD600) of *C. albicans* (ATCC 10231) in A) Sabouraud (pH 5.5) and B) LB (pH 7.4) media as a function of PVA, **CS300**, **CS7** and **CS1** concentration. The cultures were incubated at 37 °C for 18 h before the measurements. Depicted values (average ± SD) are based on 3 biological replicas.

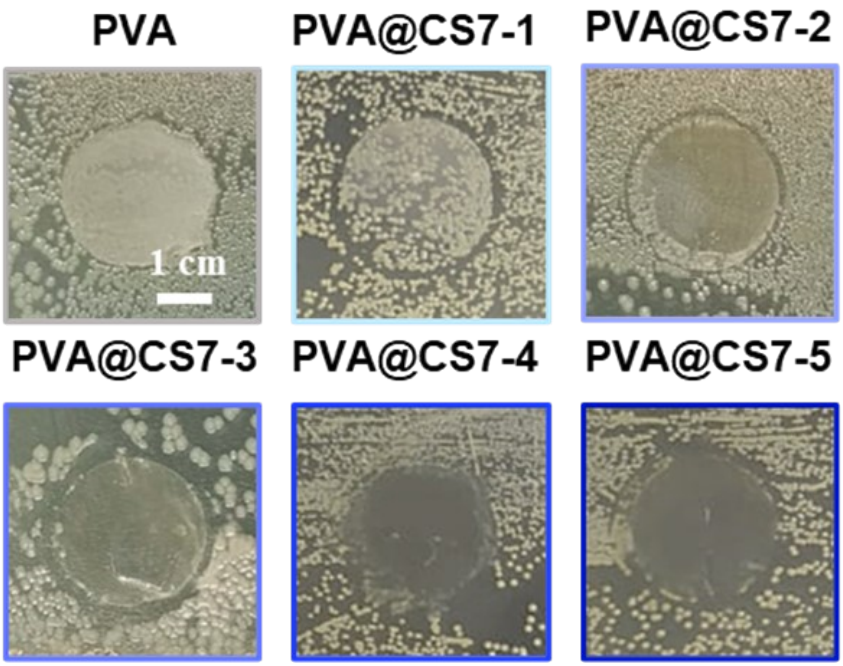

Fig. S13. Representative images of PVA@CS7 NF disks incubated overnight in agar previously inoculated with *E. coli* (K12).

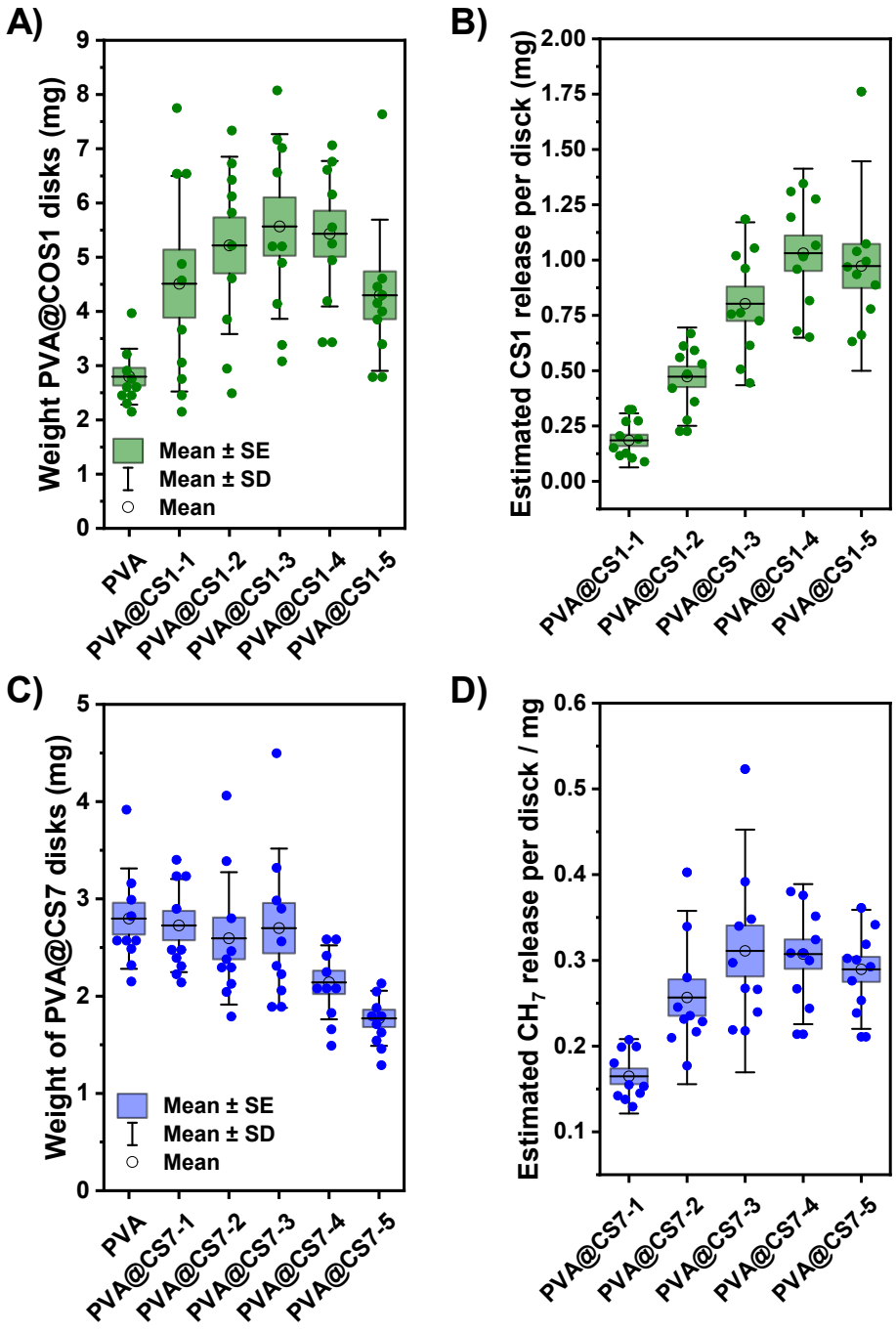

Fig. S14. Weight distribution of A) PVA@CS1 and B) PVA@CS7 NFs disks for microbial detection and estimated release from C) **CS7** or D) **CS1**.

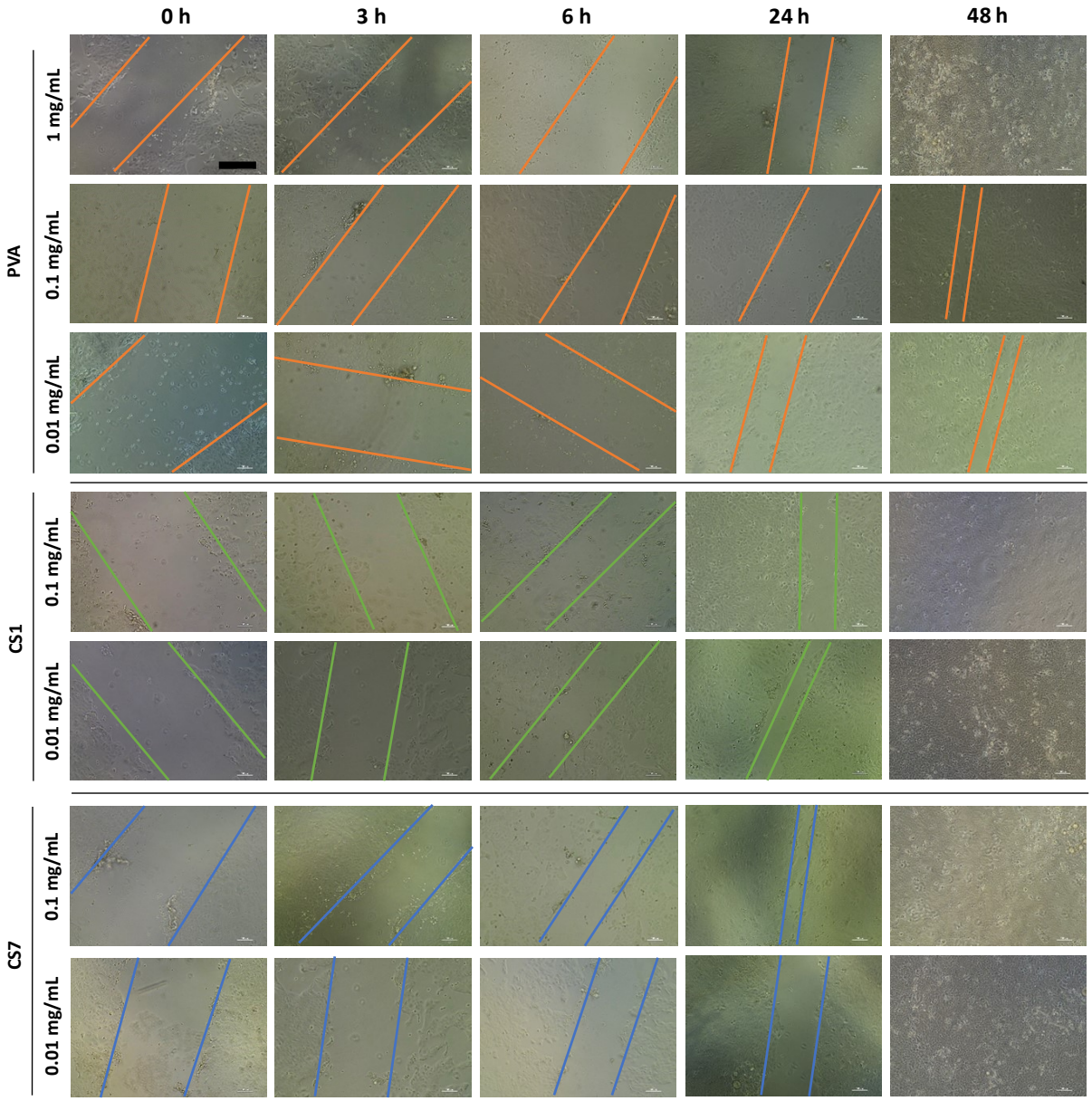

Fig. S15. Representative images of HaCaT-ras A5 cells proliferation in the presence of PVA, **CS1**, and **CS7** at different concentrations (scale bar = 200 μm).

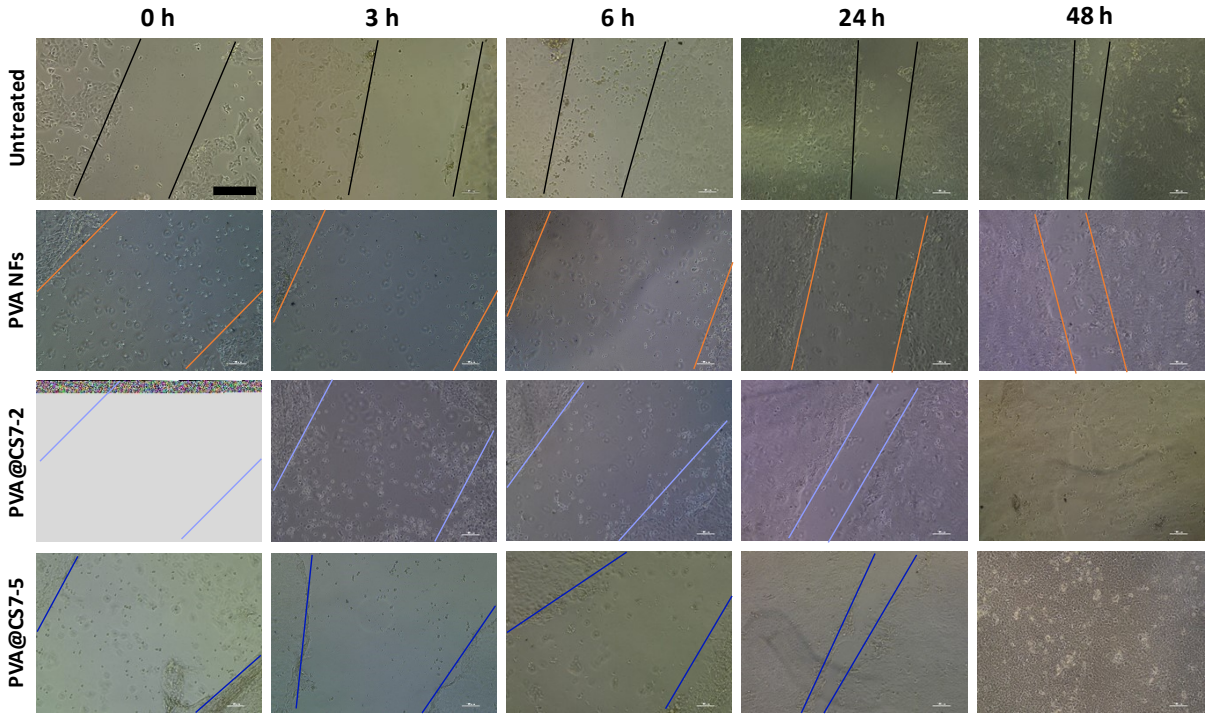

Fig. S16. Representative images of HaCaT-ras A5 cells proliferation in the absence (untreated) and in the presence of PVA and PVA@CS7 NF (scale bar = 200 μm).

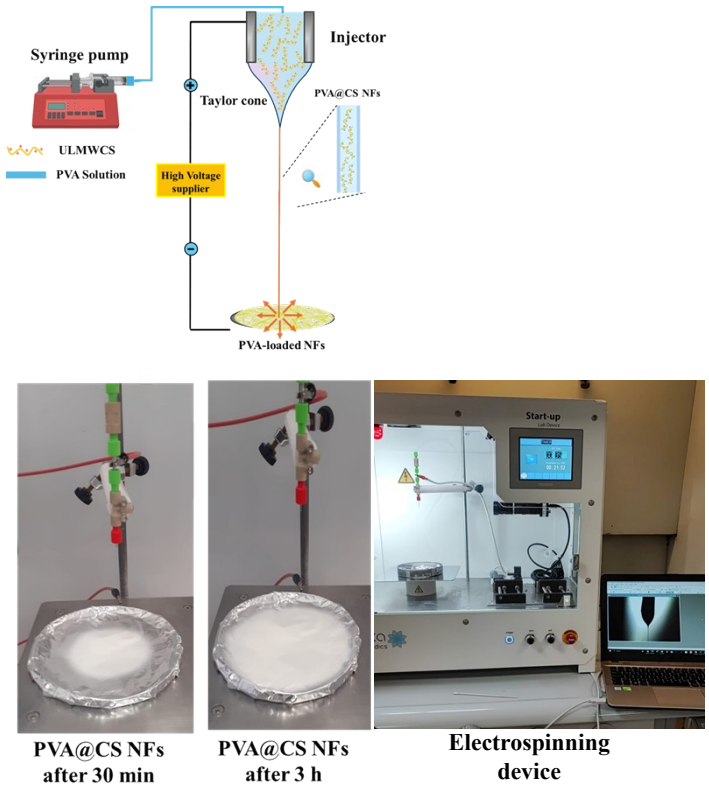

Fig. S17. Schematic representation for the fabrication of the NFs by the electrospinning including photographic images of the electrospinning process after 15 and 60 min.

4.Reference

[1] T. M. Barbosa, R. Rittner, C. F. Tormena, G. A. Morris, M. Nilsson, *RSC Adv* **2016**, *6*, 95173.

[2] D. H. Wu, A. D. Chen, C. S. Johnson, *J Magn Reson A* **1995**, *115*, 260.

[3] D. Sinnaeve, *Concepts in Magnetic Resonance Part A* **2012**, *40*, 39.

[4] F. M. Arrabal-Campos, L. M. Aguilera-Sáez, I. Fernández, *J Phys Chem A* **2019**, *123*, 943.

[5] K. Xu, S. Zhang, *Anal Chem* **2014**, *86*, 592.

[6] P. V Giampouras, K. E. Themelis, A. A. Rontogiannis, K. D. Koutroumbas, *IEEE Transactions on Geoscience and Remote Sensing* **2016**, *54*, 4775.

[7] B. Yuan, Y. Ding, G. M. Kamal, L. Shao, Z. Zhou, B. Jiang, P. Sun, X. Zhang, M. Liu, *Journal of Magnetic Resonance* **2017**, *278*, 1.

[8] F. M. Arrabal-Campos, P. Oña-Burgos, I. Fernández, *Polym Chem* **2016**, *7*, 4326.